Fluid Dynamics & Materials Processing
DOI:10.32604/fdmp.2020.010489
Article

Numerical Simulation of Retrofit Scheme of a Boiler Tail Flue

Yukun Lv, Jiaxi Yang, Jiawen Wang*, Runcheng Zhang, Shuang Yang and Wentao Li

North China Electric Power University, Baoding, 071003, China
*Corresponding Author: Jiawen Wang. Email: wangjiawenjy@163.com
Received: 06 March 2020; Accepted: 12 October 2020

Abstract: Aiming at the problem that the total pressure loss of the flue of the electric precipitator of the 350 MW unit of a power plant to the inlet of the draft fan is too large, the numerical simulation software Fluent and the standard k-ε model was used to simulate the flue, the results show that the main part of the flue mean total pressure loss is derived from the confluence header and elbow. In order to reduce the loss and consider the cost of transformation, the concept of two-dimensional feature surface is established, gradually proposed three sets of flue transformation program and analysis of the flue transformation program drag reduction effect, the results show that the total reduction of the flue can be reduced from 486 Pa to 89 Pa and the reduction rate is 81.7%, which is the best solution; The concept of two-dimensional feature plane is helpful for quick condensing of flue; Double V-type structure of the convergence of the box has a better drag reduction effect.

Keywords: Flue; numerical simulation; total pressure loss; two-dimensional feature surface; transformation program

1 Introduction

Whether the tail flue of a thermal power plant is optimized or not will not only affect the resistance of the smoke and wind system, but also affect the running state of the equipment connected to it [1–3]. A 2 × 350 MW unit of a power plant has undergone a technical transformation of two units sharing one smoke tower for smoke extraction. It is the thermal power plant with integrated smoke tower, combined setting of fan and supercharging fan, no by-pass desulfurization system and using GFRP clean flue. However, the unit #2 is in the process of reforming the fan and the supercharging fan. As a result, the drag from the outlet of the dust precipitator to the inlet of the fan is large, which affects the operation economy of the unit.

In recent years, with the development of computer technology, numerical simulation technology has gradually matured. At present, numerical simulation of flue gas in thermal power plant has been widely studied. Tajik et al. [4] employed the developed numerical framework to a higher thermal efficiency of flue-wall design modifications. Chen et al. [5] have studied the influence of two supporting schemes on the flow field of elbow in 90 rectangular ducts by using CFD. Other scholars have carried out modification studies under different conditions of unit flue [6–9].

Therefore, this paper intends to use Fluent software to simulate the flow field of the #2 unit's electrostatic precipitator outlet to the inlet section of the induced draft fan, to explore the main parts and causes of the greater total pressure loss in this section of flue. In order to reduce the total pressure loss and consider the cost of retrofitting, the concept of two-dimensional characteristic surface of flue was established. Progressively propose and simulate the drag reduction effect of three sets of flue retrofit schemes, show their comparative analysis and preferential selection process, and expect to obtain the optimal drag reduction scheme of the flue.

2 Physical Model and Numerical Calculation Method

2.1 Physical Model

After the transformation of #2 by merging induced draft fan and boost fan into one, the physical model of flue from electrostatic precipitator outlet to the inlet of the induced draft fan and the cross-section of each character are shown in Fig. 1.

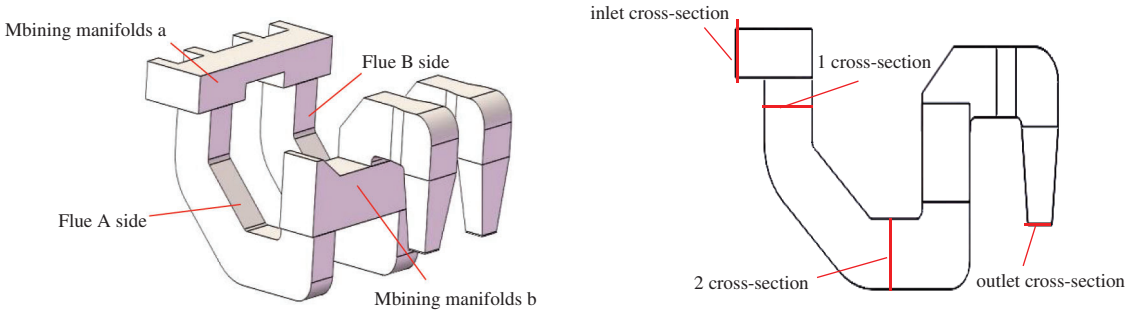

Figure 1: Physical model of the original flue. (a) Isometric view and (b) Left view

2.2 Equations and Mathematical Expressions

In Fig. 1, the flue has more elbows and shaped parts. Re at the entrance is about 1.39×10^5 around the entrance at full load, and the flow of flue gas should be three-dimensional turbulence, and the calculation area is large, the standard k-ε turbulence model is often used to study such problems [10].

Continuous equation:

$$\frac{\partial \rho}{\partial t} + \frac{\partial}{\partial x_i}(\rho \overline{u}_i) = 0 \tag{1}$$

Momentum equation:

$$\frac{\partial(\rho \bar{u}_i)}{\partial t} + \frac{\partial(\rho \overline{u_i u_j})}{\partial x_j} = -\frac{\partial \bar{\rho}}{\partial x_i} + \frac{\partial}{\partial x_j}((\mu + \mu_t) \cdot (\frac{\partial \bar{u}_i}{\partial x_j} + \frac{\partial \bar{u}_j}{\partial x_i} - \frac{2}{3}\delta_{ij} + \frac{\partial \bar{u}_l}{\partial x_l})) + \frac{\partial}{\partial x_j}(-\rho \overline{u'_i u'_j}) \tag{2}$$

Turbulent kinetic energy equation:

$$\frac{\partial(\rho k)}{\partial t} + \frac{\partial}{\partial x_i}(\rho k \bar{u}_i) = \frac{\partial}{\partial x_j}((\mu + \frac{\mu_t}{\sigma_k})\frac{\partial k}{\partial x_j}) + G_k + G_b - \rho\varepsilon - Y_M + S_K \tag{3}$$

Dissipation rate equation:

$$\frac{\partial(\rho k)}{\partial t}+\frac{\partial}{\partial x_i}(\rho k\bar{u}_i)=\frac{\partial}{\partial x_j}((\mu+\frac{\mu_t}{\sigma_\varepsilon})\frac{\partial \varepsilon}{\partial x_j})+C_{1\epsilon}\frac{\varepsilon}{k}(G_k+C_{3\varepsilon}G_b)-C_{2\varepsilon}\rho\frac{\varepsilon^2}{k}+S_\varepsilon \tag{4}$$

In Eqs. (3) and (4),

$$\mu_t=\rho C_\mu\frac{k^2}{\varepsilon} \tag{5}$$

For the area near the wall, the standard wall function method is used to correct.

2.3 Dary Condition Setting

The working medium in the flue is selected to be air with a designed temperature of 129°C, a density of 0.8599 kg/m^3, and a kinematic viscosity of 2. 204 × 10^{-5} m^2/s. The dust collector outlet (in cross-section) is set to the speed inlet boundary. At full load, the average flue gas flow is 500 m^3/s and the average speed is 14.4 m/s. The inlet of the induced draft fan (out cross-section) is set to the boundary of the pressure outlet, and the wall of the flue is considered to be the adiabatic wall.

2.4 Mesh Generation and Verification of Irrelevance

According to the space structure of that flue, the flue is meshed by hexahedral structured grid, and the quality is good after the grid quality check. After grid-independence verification (Tab. 1), the number of grids used was about 3.54 million.

Table 1: Grid independence test of the original flue

Grid density	2.69 × 10^6	2.87 × 10^6	2.99 × 10^6	3.21 × 10^6	2.38 × 10^6	3.54 × 10^6	3.82 × 10^6	4.11 × 10^6
Total pressure loss (Pa)	436.2	434.1	457.8	472.1	483.1	486.0	486.1	486.0

3 Original Flue Simulation Results

The simulation calculation is carried out on the model using the above boundary conditions, and the test total pressure, the simulated total pressure are compared. It can be seen from Tab. 2 that the error is just 8.8%. The feasibility of the simulation is proved. And the calculation results of the main cross-sections are shown in Tab. 3. Each characteristic cross-section is in Fig. 1. Fig. 2 shows the full pressure cloud diagram of the original flue.

Table 2: Comparison of test total pressure and simulated total pressure at full load

Test total pressure (Pa)	Simulated total pressure (Pa)	Error (%)
533	486	8.8

It can be seen from Tab. 3 that the total pressure loss is divided into three parts. They are total pressure loss from cross-section in to cross-section 1, total pressure loss from cross-section 1 to cross-section 2, and total pressure loss from cross-section 2 to cross-section out. Each partial pressure loss accounts for about 1/3 of the total pressure loss.

In Fig. 2, there are several low-pressure zones in the confluence box 1, which causes a certain total pressure loss, and the flue gas turns sharply downward at the exit of the confluence box 1, causing a large local loss. The above constitutes the first part of the total pressure loss. The second part of the total

Table 3: Main simulation results of the original flue

Position	Total pressure (Pa)	Mean total pressure (Pa)	Partial pressure loss (Pa)	Total pressure loss (Pa)
in1	900	889. 5	161. 5	486
in2	923			
in3	843			
in4	892			
A1	725	728	155. 5	
B1	732			
A2	618	572. 5		
B2	527			
out1	410	403. 5	169	
out2	397			

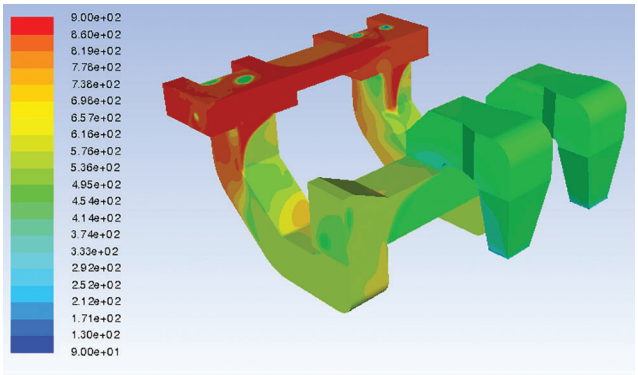

Figure 2: The original flue full pressure cloud

pressure loss is mainly caused by two elbows from cross-section 1 to cross-section 2. The total pressure loss in the confluence box 2 and the total pressure loss at the reducers and elbows constitute the third part of the total pressure loss. Therefore, the main parts and causes of the three partial pressure losses should be analyzed in detail to explore the direction of drag reduction optimization.

First, a horizontal cross-section is made along the longitudinal direction (somewhere) of the original flue confluence box 1, and is supplemented by the velocity vector diagram of the cross-section, as shown in Fig. 3.

As can be seen from Fig. 3b, there are two main vortices in the confluence box 1 corresponding to the lateral scale of the confluence box. This is due to the fact that there are speed differences between the two inlets of the adjacent inlets, and the blocking of the right-angled curved wall, and two groups of flue gas are squeezed together. The two main vortices can be eliminated or weakened.

Secondly, a vertical cross-section is made along the longitudinal direction of the original flue A side, and is supplemented by the velocity vector diagram of the cross cross-section, as is shown in Fig. 4.

As can be seen from Fig. 4b, on the original flue A side, when the flue gas flowing out of the confluence box 1 passes through three consecutive elbows without a flow guiding device, the secondary flow generated

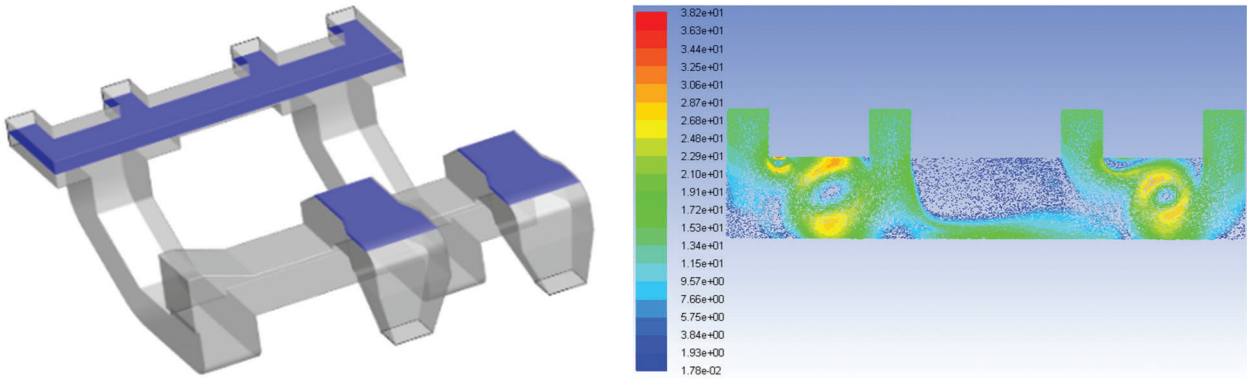

(a) (b)

Figure 3: The velocity vector of the cross section of the Mbining manifolds a. (a) Schematic diagram of horizontal cross cross-section of Mbining manifolds a and (b) Speedvector of horizontal cross cross-section of Mbining manifolds a

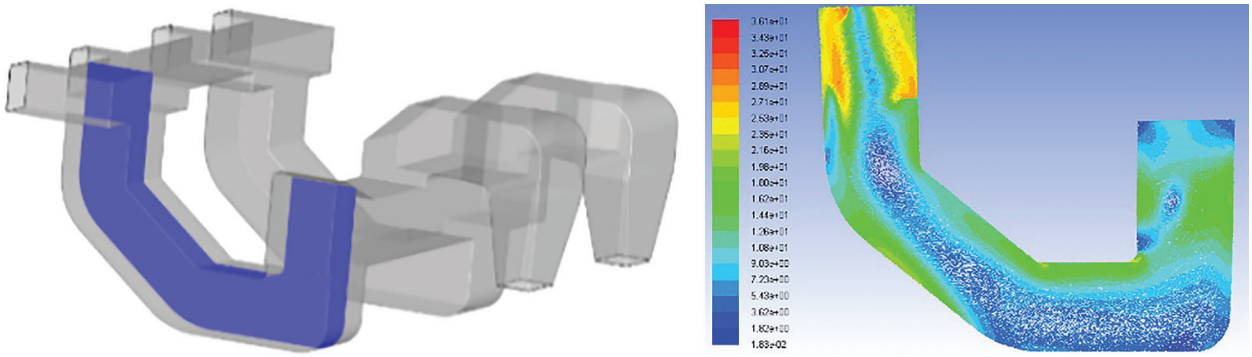

(a) (b)

Figure 4: The longitudinal cross section velocity vector of the original flue A side. (a) Drawing of Longitudinal Section of Flue A and (b) Velocity Vector of Longitudinal Section of Flue A

is continuously strengthened, in the middle of the inclined flue and the bottom of the horizontal flue, a large-scale low-speed zone is formed. Therefore, the reduction of the resistance here should be based on reducing the number of elbows.

A vertical cross-section is taken along the longitudinal direction (somewhere) of the original flue confluence box 2 and is supplemented by the velocity vector diagram of the cross-section in Fig. 5.

In Fig. 5b, there are multiple vortices in the confluence box 2 and A side flue gas squeezing the B side flue gas. And the vortex will aggravate the scouring of the inner wall by dust particles in the flue gas, causing certain safety hazards. Therefore, the necessity of confluence should be re-evaluated.

In summary, because of the extreme complexity of the original flue structure, there is no advantage in optimizing the original flue structure. The flue should be redesigned to greatly reduce the total pressure loss of confluence and elbow parts. Therefore, how to condense the transformation ideas becomes the key to the optimization of flue reduction.

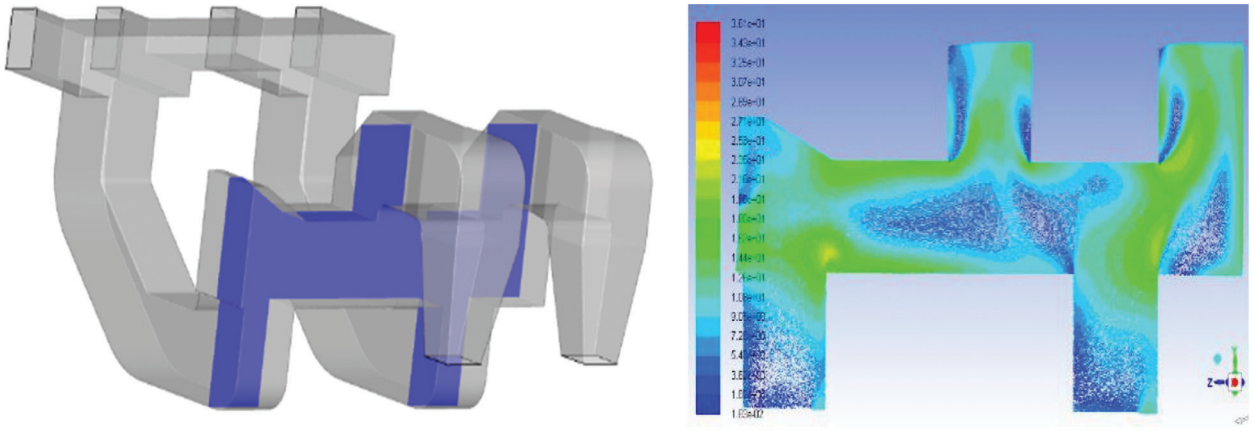

(a) (b)

Figure 5: The velocity vector of the vertical section of the Mbining manifolds b. (a) Schematic diagram of horizontal cross cross-section of Mbining manifolds b and (b) Speedvector of horizontal cross cross-section of Mbining manifolds b

4 Two-Dimensional Feature Surface Creation and Transformation Plans

4.1 Two-Dimensional Feature Surface Creation

In order to effectively propose the flue drag reduction optimization scheme, the projection of the original flue characteristic direction is first taken to obtain the two-dimensional characteristic surface of the original flue. And the center line of the characteristic surface is taken to form a straight-line segment, and get the simplified two-dimensional feature map of the original flue. Figs. 6 and 7 respectively show the left and top two-dimensional features surface of the original flue.

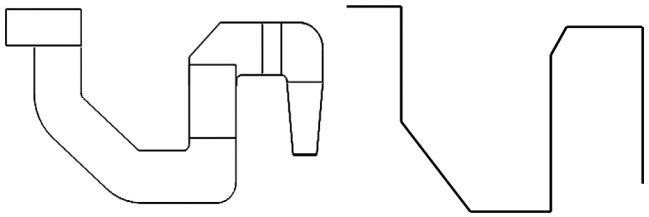

(a) (b)

Figure 6: Left sided two-dimensional feature plane. (a) Feature plane and (b) Diagram

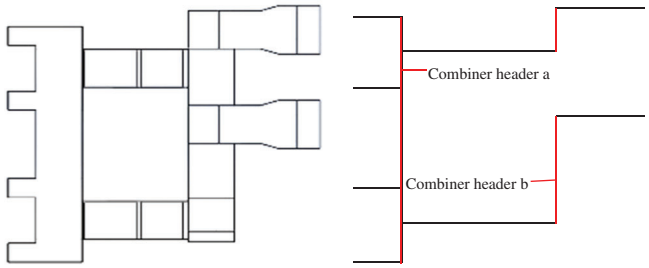

(a) (b)

Figure 7: Overlooking the two dimensional feature plane. (a) Feature plane and (b) Diagram

The original flue two-dimensional feature surface contains four 45° elbows and three 90° elbows, a total of seven elbows, as shown in Fig. 6. which is the main cause of large local resistance loss. Therefore, we should first consider reducing the number of elbows as the main optimization direction. Second, it is known from fluid mechanics [11]. The formula for calculating the local resistance loss is:

$$p_j = \xi \frac{\rho v^2}{2} \tag{6}$$

where, ξ is the local loss coefficient of the elbow. According to the research results in [12],

$$\xi = \left[0.131 + 0.163\left(\frac{d}{r}\right)^{3.5}\right]\left(\frac{\theta}{90}\right)^{0.5} \tag{7}$$

where, θ it is the bending angle, °; r is the radius of curvature of the axis, and d is the equivalent diameter of the flue. Therefore, it is known that reducing the turning angle of the elbow and turning the sharp turning elbow into a turning elbow are also effective measures for the reduction of local loss coefficient of the elbow in Eq. (7).

It can be seen from Fig. 7 and on-site investigation that the reason why the confluence box 2 is retained is due to the urgent time of its pre-reconstruction project and the expedient for rapid recovery of production. Moreover, as can be seen from the analysis of Fig. 5b, the plurality of vortices in the confluence box 2 and the squeezing of the B side flue gas by the A side flue gas exacerbate the scouring of the dust particles in the flue gas to the inner wall of the flue, caused a certain security risk, so the confluence box 2 does not have to retain. Therefore, the two-dimensional feature surface diagrams of Figs. 6 and 7 can be further optimized as is shown in Fig. 8.

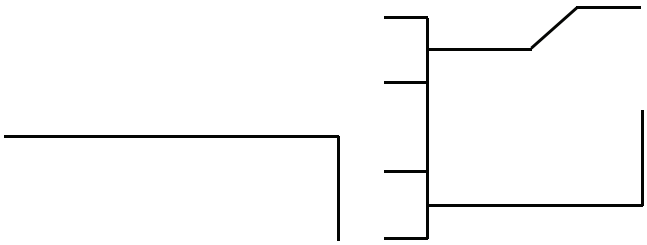

Figure 8: Optimized flue two-dimensional feature plane diagram. (a) Left view and (b) Top View

In Fig. 8b, the two 90° elbows on the original B side are changed to two 45° elbows and the two 90° elbows on the original A side are changed to a 90° elbow. After optimization, the number of elbows in the entire flue is reduced from the original 16 to 5, and $d/r \in [1,4]$. For large rectangular flue, $d/r = 1$ can be taken. Based on the optimized two-dimensional feature map of the flue, the flue transformation ideas are condensed into:

1. According to the production needs, the confluence box 1 is reserved and the outlet direction is maintained horizontal to reduce the total pressure loss caused by the flue gas turned sharply at the exit of the original confluence box 1.
2. Reduce the number of elbows from 16 to 5, and replace the two 90° elbows on the original B side with two 45° elbows to further reduce the local loss.
3. The unnecessary structure of the confluence box 2 is removed according to the current production conditions.

According to the above transformation ideas, three sets of transformation scheme are progressively designed and analyzed and compared one by one.

4.2 Transformation Scheme 1

4.2.1 Physical Model

Fig. 8 is reduced to a three-dimensional flue physics model. A flue transformation Scheme 1 (hereinafter referred to as Scheme 1) as shown in Fig. 9 is proposed. The main numerical simulation results of Scheme 1 are shown in Tab. 4.

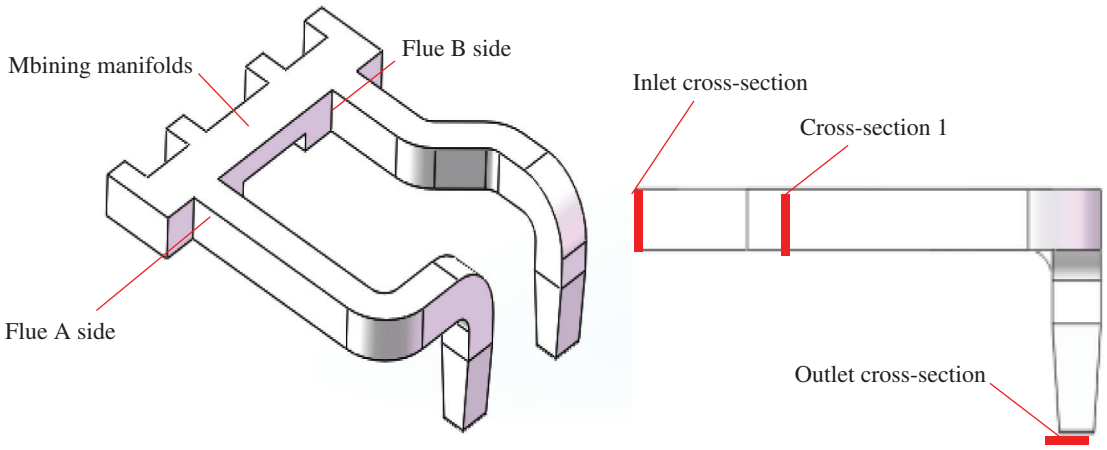

Figure 9: The physical model of Scheme 1

Table 4: The main numerical simulation results of Scheme 1

Position	Total pressure (Pa)	Mean total pressure (Pa)	Partial pressure loss (Pa)
in1	627	630	238
in2	639		
in3	638		
in4	616		
A1	451	452	
B1	453		
out1	389	392	
out2	395		

4.2.2 Simulation Results

In Tab. 4, compared with the average total pressure loss (486 Pa) of the original flue inlet and outlet, the average total pressure loss of the inlet and outlet of the Scheme 1 is only 238 Pa, which is 51% lower than the original flue. The effect is very obvious.

The average value of the total pressure of the cross-section 1 is 452 Pa. The average partial pressure loss from the inlet of the flue gas (the outlet of the electrostatic precipitator) to the outlet of the confluence box is 178 Pa, which accounts for 74% of the total pressure loss of the scheme. The elbows and reducers loss after the confluence box is 60 Pa, which is only accounts for 26% of the total pressure loss. Therefore, compared

with the original flue, the Scheme 1 is better for reducing the local resistance loss of the elbow. However, the effect of improving and reducing the loss internal the confluence box is poor. Further analysis of the Scheme 1, the Scheme 1 full pressure cloud diagram is shown in Fig. 10, and the vector diagram of the cross-section velocity along the horizontal direction of the confluence box is shown in Fig. 10.

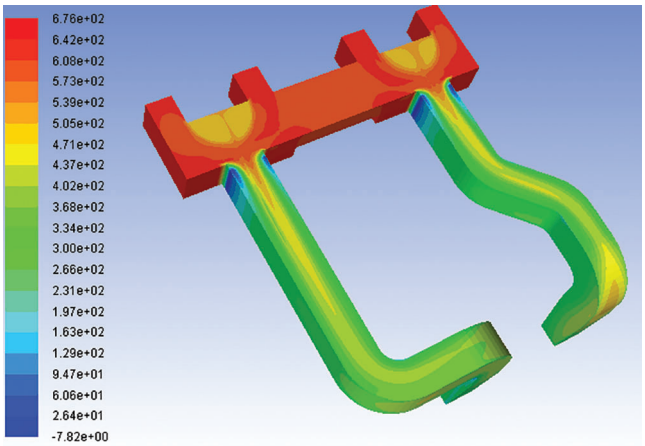

Figure 10: Program 1 full pressure cloud map

It can be clearly seen from Fig. 10 that the total pressure loss of the confluence box is large. There are two low-pressure zones obviously in the confluence box. The total pressure loss of the flue after the outlet of the confluence box is small.

Fig. 11 shows that the two flue gases in the two groups are not mutually squeezed inside the confluence box. But at the outlet of the confluence box, a large local loss is caused by the vertical cross-section contraction after the confluence. Therefore, it is necessary to consider changing the outlet structure of the confluence box to improve its internal flow field and reduce the total pressure loss of this part.

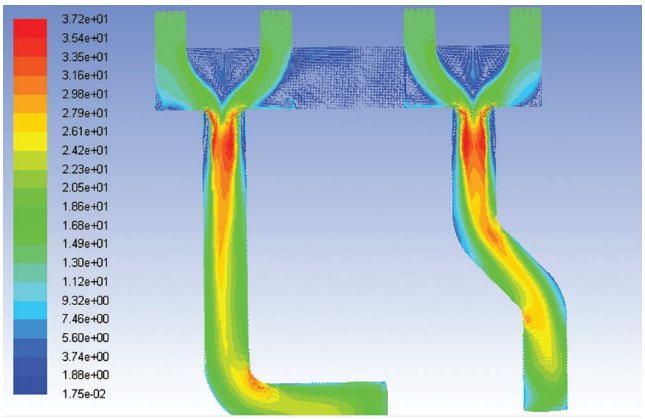

Figure 11: Scheme 1 of the confluence of the header in the horizontal direction of the cross section of the velocity vector

According to this, the outlet structure of the confluence box can be optimized. It is changed into a double V-shaped confluence box. The confluence angles are 120°, 90°, and 60° respectively, as a preliminary scheme for the transformation Scheme 2.

4.3 Transformation Scheme 2

4.3.1 Physical Model

The preliminary physical model of the transformation Scheme 2 is shown in Fig. 12. The simulation results of each confluence angle reconstruction plan are shown in Tab. 5.

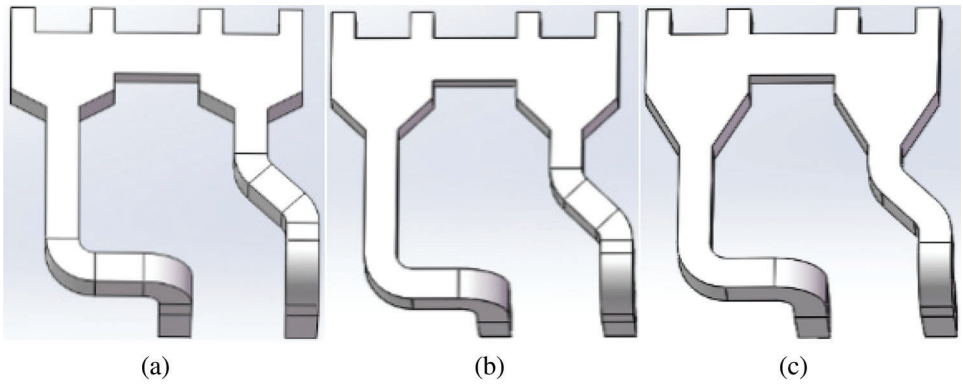

Figure 12: The preliminary scheme of double V-type Structure. (a) 120° (b) 90° and (c) 60°

Table 5: The preliminary results of the simulation

Confluence angle	120°	90°	60°
Total pressure loss(Pa)	147	125	118

In Tab. 5, as the confluence angle decreasing, the total pressure loss gradually decreases. It seems that the 60° confluence scheme is relatively superior. However, the double V-shaped structure has a relatively long length (as shown in Fig. 12), which may cause an increase in project cost. The structure will also shorten the straight pipe after the confluence box. The 90° confluence scheme has a total pressure loss of only 7 Pa higher than the 60° confluence scheme. Therefore, the 90° confluence scheme can be adopted as the transformation Scheme 2 in Fig. 13 (hereinafter referred to as Scheme 2).

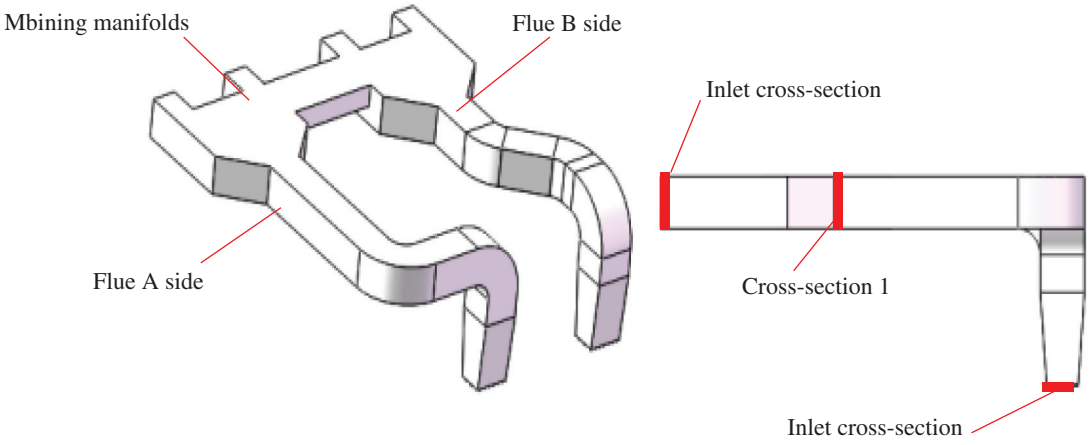

Figure 13: The physical model of Scheme 2

4.3.2 Simulation Results

The main simulation results of Scheme 2 are shown in Tab. 6.

Compared with the Scheme 1, it can be seen from Tab. 6 that the total pressure loss of the Scheme 2 is only 125 Pa. The total pressure loss is further reduced. And the partial pressure loss from cross-section in to the cross-section 1 of the Scheme 2 is only 59 Pa, which is reduced by 119 Pa. The drag reduction effect is remarkable. The partial pressure loss from the cross-section 1 to the cross-section out is 66 Pa, which is not much different from the Scheme 1.

Table 6: Numerical simulation results of Scheme 2

Position	Total pressure (Pa)	Mean total pressure (Pa)	Partial pressure loss (Pa)
in1	511	517	125
in2	522		
in3	521		
in4	514		
A1	461	458	
B1	455		
out1	391	392	
out2	393		

Further analysis of Scheme 2, the Scheme 2 full pressure cloud diagram is shown in Fig. 14. The vector diagram of the cross-section velocity along the horizontal direction of the confluence box is shown in Fig. 15.

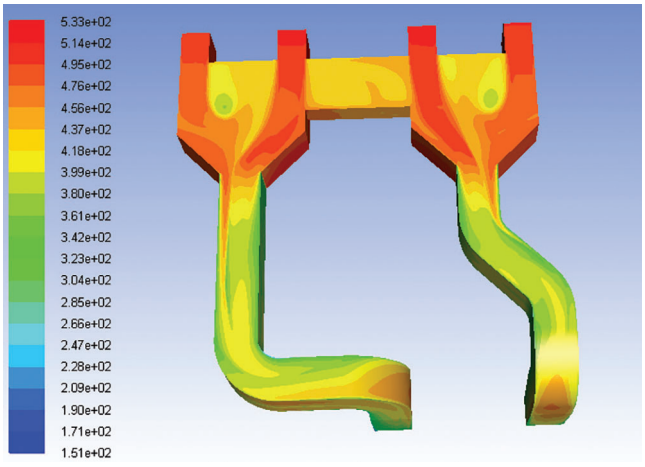

Figure 14: The full pressure cloud map of Scheme 2

Fig. 14 shows that the pressure distribution of the confluence box is more uniform compared with the Scheme 1. There is almost no mutual squeeze between the two groups of confluence, and the double V-type confluence box has diversion effect.

Comparing Fig. 15 with Fig. 11, at the exit of the double V-shaped confluence box, the confluence speed of the two flue gases is reduced. But in the flue after the confluence exit, there are still some areas where the

flue gas flow rate is high. Therefore, it is considered to increase the cross-sectional area of the flue after the confluence outlet to reduce as much as possible the flow rate of the flue gas [13].

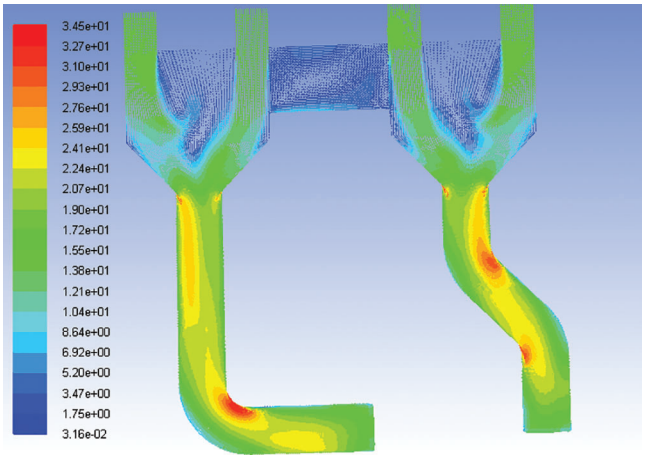

Figure 15: The velocity vector of the cross section of the Scheme 2 horizontal direction

4.4 Transformation Scheme 3

4.4.1 Physical Model

For the Scheme 2, the flue transformation Scheme 3 (hereinafter referred to as Scheme 3) shown in Fig. 16 is proposed.

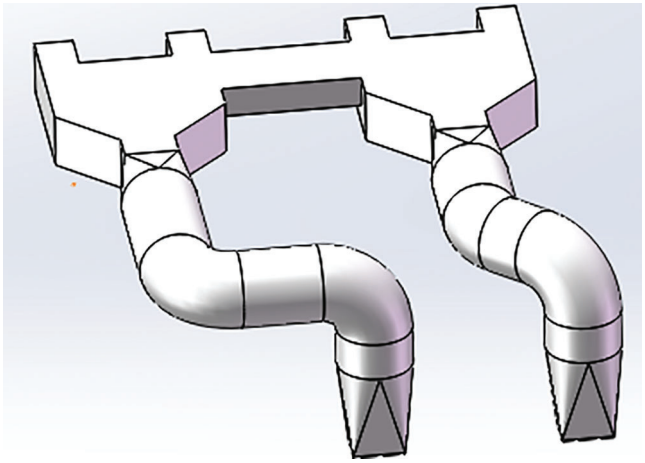

Figure 16: The physical model of Scheme 3

Compared with Scheme 2, Scheme 3 has the following improvements:

1. Using a square-round joint, the rectangular cross-section flue is transformed into a circumscribed circular flue to increase the cross-sectional area of the flue and reduce the flue gas flow rate.
2. Compared with the rectangular cross-section flue, the circular cross-section flue is flexible in arrangement. The 90° elbow can be rotated in any direction, which makes the B side flue directly connected to the confluence box. Thus two 45° elbows of the B side flue can be reduced to one.

It should be pointed out that the construction cost and construction difficulty will increase slightly with the square-round joint. The variable diameter flue structure will also increase the total pressure loss to a certain extent. The main simulation results of Scheme 3 are shown in Tab. 7.

Table 7: Main simulation results of Scheme 3

Position	Total pressure (Pa)	Mean total pressure (Pa)	Partial pressure loss (Pa)
in1	507	487. 25	89. 75
in2	484		
in3	482		
in4	476		
out1	394	397. 5	
out2	401		

4.4.2 Simulation Results

In Tab. 7, compared with the average total pressure loss (486 Pa) of the original flue inlet and outlet, the average total pressure loss of the inlet and outlet of Scheme 3 (circular cross-section flue) is only 89.75 Pa, which is reduced by 81.7%. Its drag reduction effect is optimal.

Further analysis of Scheme 3, the full pressure cloud diagram and velocity vector of Scheme 3 are shown in Fig. 17. In Fig. 17a, the pressure distribution at the confluence box is relatively uniform and the two groups of confluences barely squeeze each other. However, there is still a certain degree of total pressure loss from the outlet of the confluence box to the square-round joint. The total pressure distribution after the square-round joint is relatively uniform and the loss is small. Fig. 17b shows that the change of the flue gas flow rate is mainly concentrated at the square-round joint and elbows. The rest of the flow is relatively uniform, achieving the expected drag reduction effect.

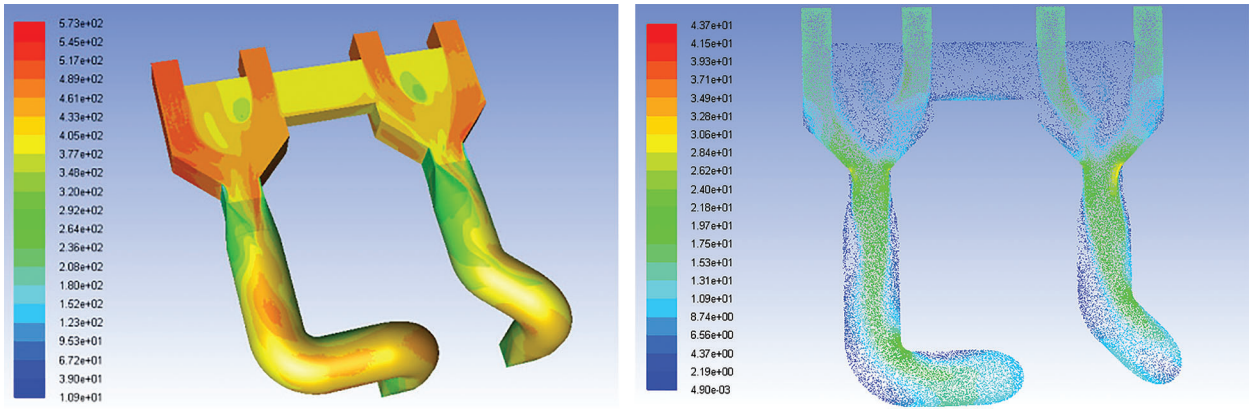

(a) (b)

Figure 17: The total pressure nephogram and velocity vector of Scheme 3. (a) Axis side total pressure nephogram and (b) Velocity vector of axis section of horizontal flu

5 Comparative Analysis of Three Sets of Transformation Schemes

The comparative analysis of the original flue scheme and the three sets of transformation schemes are shown in Tab. 8.

Table 8: Comparison and analysis of different programs

Scheme	Mean resistance (Pa)	Reduction drag relative value	Qualitative evaluation of engineering cost
Original flue	486.5	——	——
Scheme 1	238	51%, good	Construction difficulty is small and cost is small.
Scheme 2	121.8	74.9%, better	The construction is slightly more difficult and the cost is slightly higher.
Scheme 3	89.75	81.5%, optimal	The construction is difficult and expensive.

It can be seen from Tab. 8 that the Scheme 3 is optimal in terms of drag reduction effect. However, from the perspective of the cost of the renovation project, the cost of Scheme 3 may also be the largest. In addition, in the calculation of engineering quantity, the influence of factors such as flue support, induced draft fan air volume and pressure matching should be fully considered. The optimal plan that meets the requirements should be selected [14,15]. At present, considering the increasingly severe energy crisis, it is more important to reduce the pressure loss and save energy. So Scheme 3 should be chosen first.

6 Conclusion

1. The original flue total pressure loss mainly consists of three parts: Complex flow field in two combiner boxes, more elbows in the flue, the first two interactions.
2. Established and based on the concept of two-dimensional feature surface, the effect of drag reduction is obvious of Scheme 1. It is indicated that the concept of two-dimensional feature surface helps to quickly condensing ideas of flue transformation.
3. Among the three sets of transformation plans proposed by the progressive, Scheme 3 can make the average full pressure loss of the flue be reduced from 486 Pa of the original flue to 89 Pa. The drag reduction rate is 81.7%, which is the optimal scheme.
4. In the flue transformation, the full pressure loss of the confluence box should be given full attention, and the double V-shaped confluence box is better in drag reduction.

Funding Statement: The author(s) received no specific funding for this study.

Conflicts of Interest: The authors declare that they have no conflicts of interest to report regarding the present study.

References

1. Zhang, S. (2019). Thermal performance test of wind turbine in denitrification transformation of power station unit. *Electric Power Science and Engineering, 35(2),* 75–78.
2. Li, Z. G., Liu, Z. C., He, J., Na, Y. J., Lv, Q. G. (2009). Influence of entrance flue arrangement on performance of cyclone separator. *Journal of Chinese Electrical Engineering Science, 17(2),* 1–7.
3. Liu, P., Tan, Q. Y., Tang, X. S. (2010). Integrated Chimney and cooling tower, combined fan, design of flue gas system for desulfurization without by-pass flue. *Electric Power Construction, 18(3),* 74–78.

4. Tajik, A. R., Shamim, T., Zaidani, M., Abu Al-Rub, R. K. (2018). The effects of flue-wall design modifications on combustion and flow characteristics of an aluminum anode baking furnace-CFD modeling. *Applied Energy, 230 (08),* 207–219. DOI 10.1016/j.apenergy.2018.08.078.
5. Chen, G. Y., Geng, Y., Zheng, L. Y. et al. (2013). Numerical simulation of pressure loss of flue elbow in power plant with internal support structure. *Journal of Chinese Electrical Engineering Science, 28(1),* 153–159.
6. Žužek, B., Burja, J. (2017). Investigation of nickel alloy fan blade failure in a flue gas desulfurization unit. *Engineering Failure Analysis, 82(01),* 855–861. DOI 10.1016/j.engfailanal.2017.08.021.
7. Liu, M., Meng, G. X., Yan, J. J. et al. (2013). Performance diagnosis and optimization of the flow field in the flue gas dusts before the dustremoval devices of a thermal power plant. *Journal of Chinese Electrical Engineering Science, 33(11),* 1–7.
8. Wang, K., Wang, P. C. (2018). Vibration analysis and transformation of the tail flue of 350 MW supercritical circulating fluidized bed boiler. *Shanxi Electric Power, 37(5),* 53–55.
9. Yakinthos, K., Vlahostergios, Z., Goulas, A. (2003). Modeling the flow in a 90° rectangular duct using onereynolds-stress and two eddy-viscosity models. *International Journal of Protection, 19(4),* 17–19.
10. Haque, Shah, M. E., Rasul, M. G., Khan, M. M. K., Deev, A. V., Subaschandar, N. (2007). *A numerical model of an electrostatic precipitator (Ph.D. Thesis)*. School of Engineering, The University of Queensland, Australia.
11. Wang, S. I. (2007). *Fluid mechanics*. China: China Electric Power Press.
12. Pelletier, H., Krier, J., Gauthier, C. (2011). Influence of local friction coefficient and strain hardening on the scratch resistance of polymeric surfaces investigated by finite element modeling. *Procedia Engineering, 10(7),* 1772–1778. DOI 10.1016/j.proeng.2011.04.295.
13. Feng, W. (2014). A Study of local drag characteristics in elbow pipe. *Advanced Materials Research, 46(5),* 3373–3376. DOI 10.4028/www.scientific.net/AMR.955-959.3373.
14. Andrew J. E. (2019). Optimizing coronary artery calcium scanning to meet the challenges of population screening. *Journal of Cardiovascular Computed Tomography, 13(6),* 303–304.
15. Tao, W. Q. (2010). *Numerical heat transfer (Ph.D. Thesis)*. Xi'an Jiaotong University Press, China.